Size and Shape Characterization of Thermoreversible Micelles of Three-Armed Star Elastin-Like Polypeptides

Ali Ghoorchian,[†] Kaitlin Vandemark,[‡] Krista Freeman,[‡] Sumit Kambow,[†] Nolan B. Holland,[†] and Kiril A. Streletzky*[‡]

[†]Department of Chemical and Biochemical Engineering, Cleveland State University, Cleveland, Ohio 44115, United States
[‡]Department of Physics, Cleveland State University, Cleveland, Ohio 44115, United States

Ⓢ Supporting Information

ABSTRACT: Three-armed star elastin-like polypeptides are shown to have the capability of self-assembling into micellar constructs at certain environmental conditions. Here, a study of the size distribution, shape, and molecular weight of these micelles at different salt concentrations and pH values is presented. Multiangle dynamic light scattering was used to study the formation, reversibility, and size of the micelles at different environmental conditions. On the basis of the salt concentration of the solution, two distinct size distribution regimes and a transition region were observed. Static light scattering was performed to study the molecular weight and geometrical anisotropy of the micelles in each regime. The anisotropic behavior and elongation of the particles were independently confirmed by depolarized dynamic light scattering, and a model for micelles at each regime was proposed. The size and molecular weight of the micelles were verified using viscosity measurements. The results of this study suggest that there is big jump in the size and molecular weight of the micelles from the first salt-dependent regime to the other, and the shape of the micelles changes from spheres to cylindrical micelles with a higher than 10:1 axis ratio.
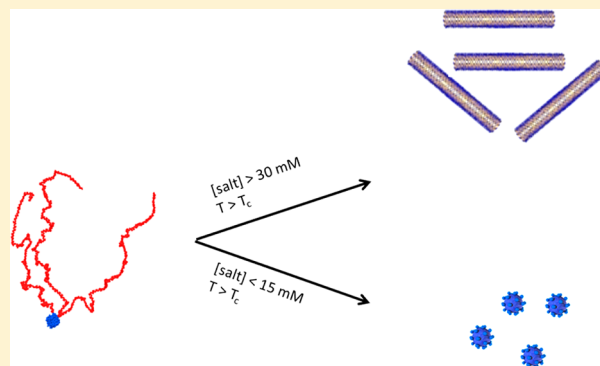
INTRODUCTION

Self-assembly of macromolecules into well-defined shapes and geometries has been studied for many years. However, during the past decade and particularly with the need for nanoscale materials for delivering drugs, genes, or other agents in the rapidly growing field of nanomedicine and targeted delivery it has received much more attention.[1−5] Use of well-defined self-assembling systems in minimizing premature drug release, maximizing drug circulation time, decreasing systemic toxicity, and increasing drug availability to the targeted organs have made them the focal point of many studies. Most of these nanoscale self-assembled particles are based on either liposomes or large polymeric molecules in the form of polymer conjugates or polymeric micelles.[6] Among these polymeric materials, micelles have been shown to have great potential for drug loading and administration.[7,8] They were introduced as potential drug delivery vehicles in the 1980s,[9,10] particularly for hydrophobic drugs with low solubility in water. They have superior characteristics in comparison with other nanoscale carriers based on their small size, relative ease of control over their physical characteristics, and high drug loading capacity. Among these physical characteristics, micelles' shape, in addition to their size, has a direct effect on the drug delivery efficiency,[11] and consequently, in every micellar system a thorough understanding of the size and shape of the micelles has practical importance when designing micelle-based drug delivery systems.

One of the promising families of micellar systems for drug delivery applications has shown to be environmentally responsive polymeric micelles, in which polymers with lower critical solution temperature (LCST) provide better control over the assembly and disassembly of the micelles under certain conditions.

An interesting approach to making responsive micellar systems is using environmentally responsive peptide-based polymers. The best known family of responsive polypeptides is elastin-like polypeptides (ELP).[12] These polymers consist of repeats of (Gly-Xxx-Gly-Val-Pro) in which Xxx can be any of the naturally occurring amino acids except for proline.[13] The chemical identity, length, and ultimately transition temperature of ELP constructs can be precisely controlled from the gene level, and their transition temperature has been shown to be affected by the length, sequence, and architecture of the polypeptides.[14−16] The ELP constructs can be designed to respond to many environmental stimuli including temperature, pH, electric field, and ionic strength, making them ideal for developing responsive biomaterials.[17−19]

Molecular self-assembly of ELP molecules to micro- and nanoscale constructs has been an area of active research in the past few years, and many research groups have tried to use this highly controllable system to develop medically applicable micellar systems by constructing di- or triblock copolymers of hydrophobic and hydrophilic blocks.[20−22] Recently, we synthesized a three-armed star ELP molecule, consisting of a trimer-forming oligomerization domain (foldon) and repeats of (GVGVP), which self-assembles into micellar particles.[23] Instead of having a bulky hydrophilic polymer block, this system utilizes the compact charged foldon domain as the hydrophilic headgroup. This increases the fraction of the micelle consisting of the hydrophobic core and hence can increase the loading capacity of them in comparison to the micelles with the same size which are made of multiblock constructs. Micelles of this system were shown to be as small as 20 nm in diameter, and the size could be controlled by adjusting the salt concentration in solution. Initial characterization of this system was primarily based on data from UV−vis spectroscopy and single-angle dynamic light scattering particle size analysis. Our results suggested the existence of spherical particles in salt concentrations up to 15 mM and two other regimes at higher salt concentrations: one between 15 and 45 mM and the third one above 45 mM.

Although our previous study provided insight into this new system and its ability to form micellar particles with predictable sizes, single-angle dynamic light scattering did not give us enough information to characterize the shape of the particles and, at times, their wide size distribution.[23] Other limitations of the previous study included the low laser power, insufficient quality of the optics in the particle-sizing instrument used, and the lack of capability for adjusting the optical parameters of the system. The purpose of the current study is to describe comprehensively the size, shape, and molecular weight of the micelles in each regime. Data from multiangle dynamic and static light scattering was used to probe the sizes of particles in each regime and to better understand their geometry. Static light scattering measurements along with polarized and depolarized dynamic light scattering were performed at different salt concentrations to determine the shape and molecular weight of the micelles in each salt regime.

MATERIALS AND METHODS

Polypeptide Preparation. The genes encoding (GVGVP)$_n$-foldon were synthesized using standard molecular biology methods as previously described.[23] The sequence encoded by the gene as confirmed by DNA sequencing (Cleveland Clinic) is MGH-(GVGVP)$_{40}$-GWPGYIPEAPRDG-QAYVRKDGEWVLLSTFL. The (GVGVP)$_{40}$-Foldon gene was expressed and purified with yields between 100 and 200 mg/L as previously described.[14]

The purity of the sample and its molecular weight were confirmed by SDS-PAGE gel and ion-spray quadropole/time-of-flight mass spectroscopy (AB/Sciex), respectively. The (GVGVP)$_{40}$-Foldon construct has a molecular weight of 60.3 kDa in its stable trimeric form.

Sample Preparation. Samples for measurement were made by diluting the PBS stock solutions in reverse osmosis purified water (Millipore, 18.2 MΩ-cm). Salt concentration was adjusted by adding NaCl solution from a 5 M stock solution to the desired concentration. The pH of the samples was then adjusted using 1 M NaOH solution. To make sure that the pH had stabilized, samples were left at room temperature after

initial pH adjustment for at least 30 min and the pH was measured again and, if necessary, adjusted to the desired pH value. Samples were then filtered using 0.22 μm filters (Milex-GV, 0.22 μm, Millipore) into borosilicate glass cuvettes. Cuvettes were cleaned prior to use by soaking the cells for 30 min in concentrated sulfuric acid and then for 10 min in a strong oxidizing solution containing 2 M NaOH and 0.2 M KMnO$_4$. Cells were then rinsed by water and dipped into a dilute HCl solution several times before a thorough rinse with deionized water and were dried using ultra-high-purity nitrogen gas (99.9%). A fresh sample was loaded into a newly cleaned cuvette for each measurement.

Light Scattering. Static and dynamic light scattering experiments were done using an Ar$^+$ Spectra Physics 2017 laser with a wavelength of 514.5 nm and maximum power of 2 W. A TSX-1A variable neutral density filter (ORIEL) and a VPH-4 optical iris (NRC) were used to control the laser power. The laser beam was directed onto the sample in a BI-200SM Goniometer (Brookhaven Instruments) using a series of mirrors. The sample cell was held in a decalin-filled quartz vat, and the temperature of the cell was controlled using a HAAKE-A81 refrigerated water bath ($\pm$0.2 °C). Dynamic light scattering (DLS) experiments were carried out at scattering angles from 40° to 145° in increments of 5−15°. Scattered light was detected by a BI-DS2 photomultiplier and analyzed with BI-9000 digital correlator.

DLS analyzes fluctuations in intensity (I) of the scattered light through measured intensity−intensity correlation function $S(q,\tau)$

$$S(q, \tau) = \int_0^T I(q, t)I(q, t + \tau)\,\mathrm{d}t \tag{1}$$

where q is the scattering momentum transfer vector, τ is the delay time, and T is the duration of the experiment. The magnitude of the scattering vector is

$$q = \frac{4\pi n}{\lambda_0}\sin\left(\frac{\theta}{2}\right) \tag{2}$$

Here n is the refractive index of the solvent, θ is the scattering angle, and λ_0 is the wavelength of the light in vacuum. Measured spectra $S(q,t)$ were analyzed by the line shape analysis method,[24] in which the intensity correlation function is converted to a field correlation function $g^{(1)}(q,t)$ by the Siegert relation and then fit to a sum of stretched exponentials using a nonlinear least-squares simplex algorithm[25]

$$g^{(1)}(q, t) = \sum_{i=1}^N A_i\exp(-\theta_i t^{\beta_i}) \tag{3}$$

Here N is the number of observed relaxation modes labeled by i, θ_i is the decay pseudorate, β_i is the stretching parameter, and A_i is the amplitude of a corresponding mode. Most of the data were fit with either one or two modes.

$g^{(1)}(q,t)$ can also be expressed as the Laplace transform of the normalized distribution of decay rates $A(\Gamma)$

$$g^{(1)}(t) = \int_0^\infty d\Gamma A(\Gamma)\exp(-\Gamma t) \tag{4}$$

Analysis of the correlation function can then yield mean relaxation times ($\tau = \langle\Gamma^{-1}\rangle$) of the most prominent modes. Spectral time moment analysis was applied in this study to determine the zeroth time moment for the ith mode by obtaining the mean decay rate Γ_i for that mode.[25] The apparent

mean diffusion coefficient D_i corresponding to each mode can then be calculated from each mean decay rate Γ_i as

$$D_i = \Gamma_i/q^2 \qquad (5)$$

Spectral time moment analysis allows for calculation of the mean diffusion coefficient of each mode from an accurate fit of $g^{(1)}(q,t)$. The approach considers the properties of each observed mode in detail, helping to identify physical processes corresponding to this mode. The specific methodology, applications, and advantages of this method over inverse Laplace transform-based methods are described elsewhere.[24,26]

Depolarized DLS measurements were performed using the optical system described above with a Precision Linear Polarizer (Newport 20LP-VIS-B) inserted between the scattering cell and the PMT. The incident laser light was vertically polarized, which was ensured by sending it though Glan-Laser calcite polarizer (Thorlabs, GL10). Inserting a vertical polarizer into the system resulted in a 3−5% decrease in the intensity of the scattered light for isotropic latex spheres. The polarizer was rotated by 90° between vertical (VV, or polarized) and horizontal (VH, depolarized) measurements of the scattered light.

To determine the mean translational (D_T) and rotational (θ_R) diffusion coefficients from polarized and depolarized dynamic light scattering, measured spectra were analyzed using spectral time moment analysis described above to obtain the mean decay rates ($\langle\Gamma_i\rangle_{VH}$ and $\langle\Gamma_i\rangle_{VV}$) of the correlation functions for the horizontally (VH) and vertically (VV) scattered light.

The mean translational (D_{Ti}) and mean rotational (θ_{Ri}) diffusion coefficients are then determined from the corresponding $\langle\Gamma_i\rangle$ vs q^2 for VV and VH data using

$$\langle\Gamma_i\rangle_{VV} = D_{Ti}q^2 \qquad (6)$$

and

$$\langle\Gamma_i\rangle_{VH} = D_{Ti}q^2 + 6\theta_{Ri} \qquad (7)$$

In static light scattering (SLS) experiments the angular dependence of the reduced time-average scattering intensity, known as the excess Rayleigh ratio, R_{vv}, was measured. SLS measurements were carried out with the same optical system as DLS measurements but with a smaller angular step. SLS data are analyzed typically by a Zimm plot. In cases of significant nonlinearity of the Zimm plot, a Berry plot equation is used for the extrapolation. For a dilute solution of concentration c, the Berry equation can be written as

$$\left(\frac{Kc}{R_{vv}}\right)^{1/2} = \left(\frac{1}{M_w}\right)^{1/2}\left(1 + \frac{\langle R_g^2\rangle q^2}{6} + A_2 M_w c + ...\right) \qquad (8)$$

Here, $K = 4\pi^2 n^2(dn/dc)^2/(N_A\lambda_o^4)$, dn/dc is the differential refractive index increment of the solution, N_A is Avogadro's number, M_w is the weight-average molecular weight, $\langle R_g\rangle$ is the z-average root-mean-square radius of gyration, and A_2 is the second virial coefficient. The concentration of particles in our study was low, making the effects of A_2 negligibly small. Therefore extrapolation to zero concentration was unnecessary. Extrapolation to zero scattering angle yielded the apparent M_w, while the fit of the angular dependence of $Kc/R_{vv}(q)$ produced an apparent R_g.

In order to reliably obtain the molecular weight from static light scattering measurements the differential refractive index

increment (dn/dc) of the solutions was measured directly. A Brice−Phoenix differential refractometer with split sample cell controlled by a Thermo RTE-7 refrigerated bath/circulator was used for dn/dc measurements. The values of the measured dn/dc under different conditions can be found in the Supporting Information.

Viscosity Measurements. A Cannon-Ubbelohde Semi-Micro viscometer size 25 (Cannon Instrument) was used to measure the viscosity of $(GVGVP)_{40}$-foldon solutions at different protein concentrations. The viscometer was calibrated using pure water, and measurements were carried out in a temperature-controlled (±0.1 °C) water bath (VWR, model 1122S) set up in a cold room (4 °C), allowing measurements at temperatures below room temperature. At each temperature the sample in the viscometer was equilibrated for at least 10 min. The flow of the solution through the capillary was recorded using a commercially available video camera, and flow time was recorded from the time stamp of the recording. Buffer solution and polypeptide solutions were measured at each temperature to obtain the specific viscosity. The intrinsic viscosity at temperatures above the critical micelle temperature was measured by extrapolating the specific viscosity of the solutions at different concentrations to zero concentration as described in the literature.[27]

TEM Imaging. Transmission electron microscopy was done on a FEI Tecnai G_2 Twin instrument (Eindhoven, Netherlands). A 5 μL amount of the samples was heated to 50 °C along with the TEM grids. Samples were then dried on the grid for about 5 min and the extra solution was wiped off the grid. Grids were then imaged at 160 kV and a range of magnifications.

■ RESULTS

Dynamic Light Scattering. We performed dynamic light scattering measurements at different temperatures on a 10 μM $(GVGVP)_{40}$-foldon solution with a salt concentration of 10 mM (Figure 1) to confirm temperature-induced formation of micelles and reversibility of the micellization process, as previously observed.[23] Significantly bimodal correlation func-
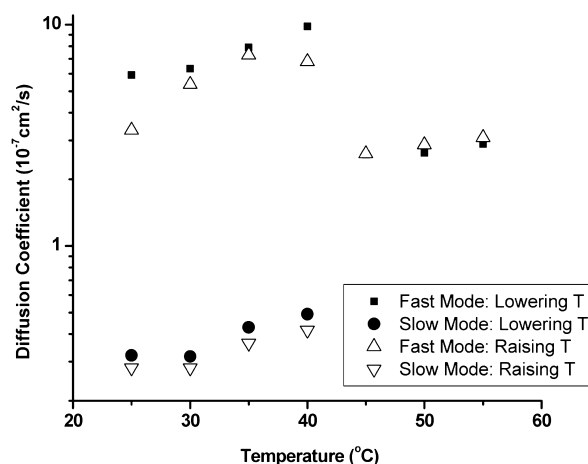

Figure 1. Measured diffusion coefficients as a function of temperature for a 10 μM solution of $(GVGVP)_{40}$-foldon at pH of 10.2 and a salt concentration of 10 mM. Two apparent diffusion coefficients (fast and slow) seen below the transition and only one (fast) above the transition. Data obtained by lowering (filled points) and raising (open point) the solution temperature.

tions were measured below the transition temperature. The faster mode (with $D = 5–9 \times 10^{-7}$ cm^2/s) was found to have a small standard deviation and no dependence of apparent diffusion coefficient on scattering angle, indicative of small diffusive particles with an apparent hydrodynamic radius (R_h) of about 3–5.5 nm, which is in agreement with our previous findings.[23] The slower mode ($D = 1–10 \times 10^{-8}$ cm^2/s) was not seen previously but had a significant contribution to the measured correlation function (amplitude of 75–85%) and stretching parameter $\beta = 0.6–0.7$, indicating either a significant polydispersity of the scatterers or contributions of various internal modes. Estimates of hydrodynamic radius for this slow mode are somewhat misleading, as this mode was found to have a strong dependence of D on scattering angle (which is atypical for center of mass diffusion of a particle). This mode is indicative of either polydispersity or various slower processes in the system such as relaxation of unfolded trimers. The different angular dependence of the observed two modes argues against averaging the two processes into one.

Above the transition temperature, only a single mode was observed at a salt concentration of 10 mM. Using a second mode at high temperatures could not be justified as the RMS error did not change significantly with addition of the second mode to the fit. The diffusion coefficient of the single observed mode ($D = 2–3 \times 10^{-7}$ cm^2/s) was found to be independent of scattering angle.

Transition temperature experiments were repeated at least three times, and data points are shown to be in very good agreement from one experiment to another. The reversibility of the micelle formation process was confirmed by showing that the diffusion coefficients corresponding to the experimental modes observed during formation of micelles upon increasing temperature are similar to the diffusion coefficients seen during disassembly of micelles with decreasing temperature (Figure 1).

The pH dependence of the micelle formation process was investigated by measuring the apparent size of micelles formed as a function of pH at constant salt concentration. A series of 10 μM protein samples with 40 mM salt was studied from pH 9.6 to 11.5 (Supporting Information). The results show an increase in diffusion coefficient (D) of the micelles with increasing pH up to pH 10.2, above which a fairly constant D was observed. On the basis of these results all of the following measurements were made after adjusting the protein solutions to pH 10.2–10.4.

The DLS correlation functions of micelles formed above the transition temperature were carefully studied at different scattering angles to further investigate the size and shape of micelles. Experiments were performed in a range of salt concentrations from 5 to 60 mM. At all salt concentrations, the normalized correlation functions of (GVGVP)$_{40}$-foldon solutions cover 2–2.5 orders of decay, signifying a good dynamic range of the experiments (Supporting Information). Comparing the normalized correlation functions at 50 °C (above the transition temperature), it is apparent that the salt concentration has a strong effect on the system. The low-salt regime data (up to 15 mM) shows nearly identical correlation functions, indicating constant apparent size. A similar clustering of correlation functions is observed in the high-salt concentration regime (30 mM and above) with much slower decay rates, corresponding to particles of larger apparent size. Between the two regimes, a region of transition is observed.

Estimates of the diffusion coefficients for different salt concentrations were obtained using two different analyses

(Figure 2): from single-angle experiments at 90° and multiangle measurements. In both cases either one- or two-mode fits were
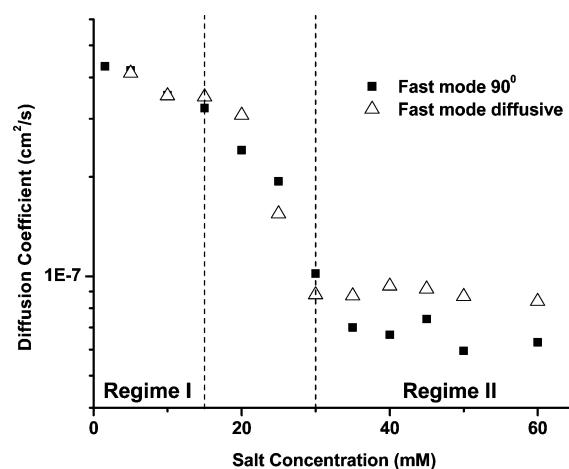

Figure 2. Measured diffusion coefficient as a function of salt concentration for a 10 μM solution of (GVGVP)$_{40}$-foldon at 50 °C. Diffusion coefficients were obtained in two ways: from the fast mode of the two-mode fit of single-angle (90°) measurements (triangles) and the q^2 dependence of the decay rate Γ of the fast mode from multiangle measurements (squares).

used. For the multiangle measurements, diffusion coefficients were obtained from the slope of q^2 dependence of decay rate Γ_t. For these measurements, only the faster of the observed modes was found to exhibit diffusive-like behavior or linear dependence of Γ_t vs q^2 at all salt concentrations; therefore, only the fast mode result is reported in Figure 2. When single-angle (90°) measurements were analyzed with two modes, two apparent diffusion coefficients were obtained. Only the faster mode of the two is reported in Figure 2.

Diffusion coefficients above the transition temperature at different salt concentrations show two distinct salt concentration regimes, as previously reported,[23] but with improved concentration resolution: a transition region is now observed between the two regimes (Figure 2). The first regime corresponds to less than 15 mM salt, and the second regime corresponds to a salt concentration range of 30–60 mM. In both regimes, the diffusion coefficient decreases only slightly with increasing salt concentration. A significant decrease in the diffusion coefficient (presumably caused by an increase in the micelle size) is observed in the transition region between the two regimes. At low salt, the relative agreement between values of D for the fast mode of 90° measurements and D from multiangle measurements for the fast mode indicates relative monodispersity and the isotropic nature of scatterers in the first salt regime. On the other hand, at high salt concentration there is a significant difference between D for the fast observed mode of 90° measurement and D for the fast mode of the multiangle measurement. This result is indicative of significant polydispersity of the scatterers or/and their optical anisotropy.

The diffusion coefficient can be used to calculate the corresponding hydrodynamic radius (R_h) of the particles using the Stokes−Einstein equation

$$R_h = \frac{k_B T}{6\pi D \eta} \tag{9}$$

where k_B is Boltzmann constant, T is the temperature, and η is the solvent's viscosity. Equation 9 is derived for a suspension of

dilute, spherical, monodisperse particles in a small molecule solvent. Our system is comprised of dilute particles in a small molecule solvent; however, one cannot *a priori* assume the monodispersity of the system or the spherical shape of the micelles. Therefore, eq 9 yields an apparent hydrodynamic radius. On the other hand, light scattering measurements at various scattering angles help to ascertain better the meaning of the apparent R_h. In particular, monodisperse spherical particles yield the decay rate of a correlation function that scales linearly with the square of the scattering wave vector q with zero intercept.

Representative angular dependences for the two salt regimes and the transition region are presented in the form of decay rate as a function of scattering wave vector squared (Figure 3a–c). A one-mode fit gives a linear dependence of Γ on q^2 with a small intercept, corresponding to an apparent radius of 13.2–15.5 nm. The two-mode fit of the correlation functions in the first regime of Figure 3a yields two nearly linear dependences of Γ vs q^2 with small intercepts. Addition of the second mode to the one-mode fit in analyzing the data does not change the RMS error of the fit significantly. The two-mode parameters have similar angular dependence to the one-mode fit results, yielding apparent sizes that average to a value similar to a single-mode fit radius. This indicates that the observed particles have a somewhat broad distribution of sizes but still on average behave as largely spherical micelles with a radius of 13.2–15.5 nm. These sizes are in agreement with previously reported sizes for this regime.[23] The spherical shape of these particles is also confirmed by depolarized dynamic light scattering in which no significant signal was detected from the micelles at low salt concentrations.

For the transition region, the plot of Γ vs q^2 shows a linear dependence of decay rate on q^2 for the first mode (with a small intercept) and somewhat different behavior for the second mode (Figure 3b). In fact, for the second mode, there is some deviation from the linear Γ vs q^2 dependence at large q, which is an indication of possible micelle geometrical anisotropy in this regime. The nonlinearity of the second mode is noticeable but not as strong as at higher salt concentrations.

In high-salt concentration regime, for single-mode fits, Γ vs q^2 shows even more significant nonlinearity at high angles (above 100°) (Figure 3c). This nonlinearity becomes more prominent with an increase in salt concentration. The data at high salt concentrations clearly had to be analyzed with two modes due to the significant bimodality of measured correlation functions. The faster of the two modes is somewhat diffusive (linear Γ vs q^2 with significant non-zero intercept), yielding micelles with an apparent hydrodynamic radius of about 45–63 nm. This mode does not change with increasing salt concentration (Figure 2). On the other hand, the slower observed mode is completely nondiffusive, as seen from a lack of strong angular dependence of the decay rate (Figure 3c) and the values of the stretching exponent ($\beta = 0.6$–0.85).

Static Light Scattering (SLS). A series of static light scattering (SLS) measurements was carried out at different salt concentrations to further investigate the size, shape, and apparent molecular weight of the micelles. The average intensity of scattered light (I) was measured at a wide range of angles and the solvent scattering under identical conditions was subtracted from it. The angular dependence of this intensity I was analyzed using the Berry equation (eq 8), instead of the Zimm equation due to some apparent curvature seen in $(I)^{-1}$ vs q^2 at high salt concentration (Supporting
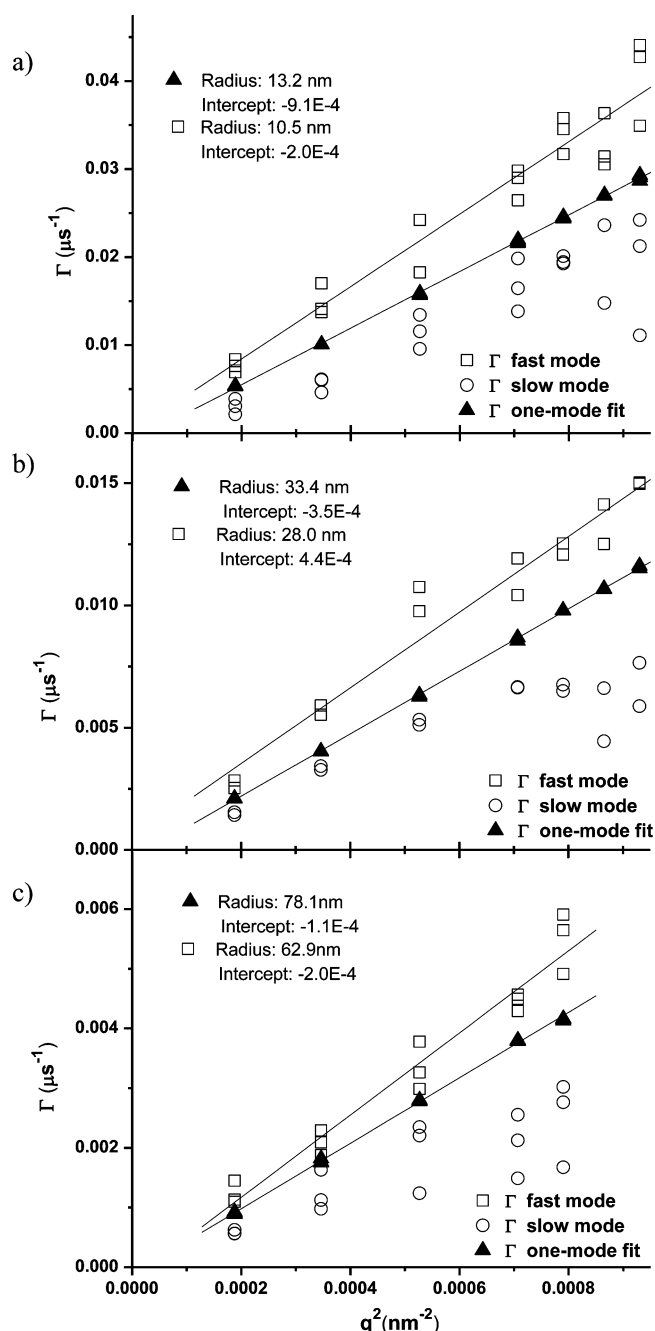

Figure 3. DLS measured decay rate (Γ) as a function of q^2 for micelles at 50 °C in two different salt concentration regimes and the transition region: (a) low-salt regime or Regime I (5 mM); (b) transition region (25 mM); (c) high-salt regime or Regime II (60 mM).

Information). The radius of gyration, R_g, was obtained from the curvature of I vs q^2 dependence.

$(I)^{-1/2}$ vs q^2 (Supporting Information) above the transition shows very little (if any) angular dependence at low salt concentration (below 20 mM), which indicates that particles present under those conditions are too small ($<\lambda/20$) to show significant dependence on scattering angle in the studied q range. On the other hand, both in the transitional region and in the high-salt concentration regime the angular dependence is strong, indicating the presence of larger particles.

Values obtained for R_g using Berry fits range between 16.8 and 111.5 nm (listed in the Supporting Information). The

dependence of R_g on salt concentration is very similar to that of R_h; both apparent sizes slightly increase with salt concentration up to 15 mM, change 4-fold in the transition region ($15 < c < 30$ mM), continue to slightly increase with concentration in the second concentration regime, and show some increase in size above 45 mM. The ratio of R_g to R_h was found to increase from about 1.1 at low salt concentration to about 1.4 at high salt concentration, indicating some elongation of the observed particles. In these calculations the apparent R_h of the dominant mode of the bimodal DLS data was used.

Extrapolation to zero scattering angle, measurement of the scattering by the standard (toluene), and direct measurement of the differential refractive index increment (dn/dc) of the solutions allowed us to calculate the apparent molecular weight, M_w, of the micelles at different salt concentrations (Figure 4
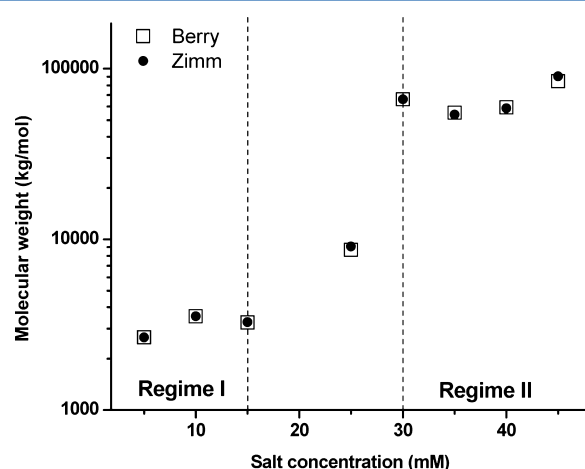

Figure 4. Apparent molecular weight as a function of salt concentration deduced from SLS data for $(GVGVP)_{40}$-foldon micelles at 50 °C using Zimm and Berry analysis. Same two salt concentration regimes and the transition region are observed.

and graph and data in Supporting Information). The dependence of M_w on salt concentration is consistent with differences in D observed in the different salt regimes (Figure 2), namely, in Regime I, M_w has little concentration dependence ranging between 2700 and 3500 kDa, while in the transitional region, M_w increases to about 66 000 kDa as the salt concentration increases from 15 to 30 mM. In Regime II, M_w is largely constant, only slightly increasing to 85 000 kDa at higher salts.

Polarized and Depolarized Dynamic Light Scattering. Polarized and depolarized dynamic light scattering experiments were carried out to study the extent of elongation of the micelles in each salt regime under conditions similar to unpolarized dynamic light scattering experiments. Incident light was vertically polarized. In Regime I, only vertically polarized scattered light (VV) was observed, with no signal observed for horizontally polarized scattered (VH) light. For higher salts, the VH signal was observed but at a much lower intensity than the VV signal with identical optical settings, yielding a depolarization ratio of 0.01 or lower. This means that previously reported unpolarized DLS scattering, which consists of both VH and VV components, was essentially the VV scattering. Still, the VH signal was strong enough to provide reliably measured correlation functions (up to 2 orders of magnitude of decay), indicating noticeable elongation of the particles (Supporting Information). The relationship between Γ and q^2 for both VH

and VV scattering showed (Figure 5) a largely linear dependence with a similar slope (especially if only low q VV
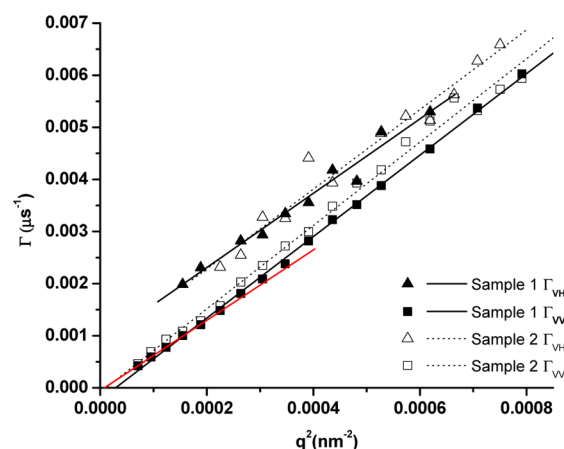

Figure 5. Decay rates Γ_{VV} (squares) and Γ_{VH} (triangles) as a function of q^2 from DDLS measurements on micelles at a salt concentration of 42 mM (open symbols, Sample 2) and 43 mM (filled symbols, Sample 1) at 50 °C. Corresponding linear fits to the data are shown as well, including a linear fit to VV data of Sample 1 at low q.

data is considered). The slopes of VV and VH decay rates and the intercept of the VH decay rate were used to calculate translational and rotational diffusion coefficients of the micelles based on eqs 6 and 7.

Viscosity Measurements. On the basis of the viscosity measurements of $(GVGVP)_{40}$-foldon solutions, the intrinsic viscosity above the T_t was calculated to be 3.356 mL/g. Experiments were performed at 40 °C or greater for solutions of protein ranging from 200 to 900 μM and salt concentration of 7.5 mM (Supporting Information). Assuming spherical micelles, the polypeptide density, ρ, within the hydrodynamic volume of the micelles can be determined from the intrinsic viscosity using[27]

$$\rho = \frac{5M_w}{2[\eta]} \tag{10}$$

This equation is derived from the well-known Einstein equation which relates viscosity to the volume fraction of spherical particles. The density of protein is also a function of protein mass and the volume fraction of the polypeptide. The volume fraction then relates the Einstein equation to the polypeptide density resulting in eq 10. The polypeptide density in the micelles is calculated to be 0.302 g/cm^3.

TEM Imaging. In an attempt to independently verify the structure of the micelles, transmission electron microscopy was used to image micelles on the surface. All samples were imaged in the same salt and pH conditions as the light scattering experiments. The results from samples in the low-salt regime (Regime I) showed clear formation of spherical micelles even after drying the samples (Figure 6). Particles are in the range of 20−30 nm in diameter as expected. This shows the very stable nature of these micelles such that even after fast drying on the TEM grid they preserve their overall morphology. Images of micelles at the high-salt regime (Regime II) showed distinguishable differences to the images at low salt concentration, but these images were not conclusive enough, which can very well be a result of the less stable nature of these elongated micelles in comparison to the spherical ones and the
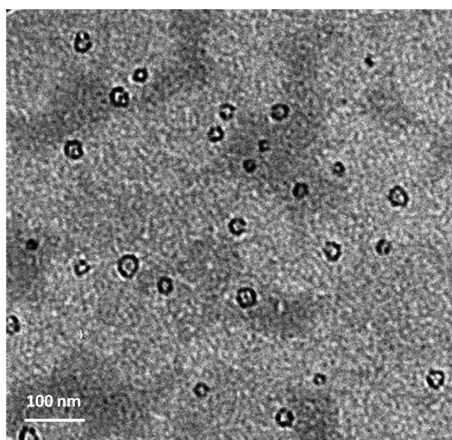
Figure 6. TEM images of micelles at low (10 mM) salt concentrations at pH 10.2. Images show well-defined spherical micelles in the range of 20−30 nm in diameter.

fact that dehydration of these less stable micelles during the drying process can change their morphology (data not shown).

■ DISCUSSION

Micelle Formation and Characterization. On the basis of our findings from dynamic and static light scattering and capillary viscometry together with previously reported data,[23] the structure of micelles formed in different salt concentration regimes can be elucidated. On the basis of the amphiphilic structure of the polypeptide it is expected that the hydrophobic ELP makes up the core and the charged foldon acts as the headgroup to form the surface of the micelles. Geometric changes of these components based on solution properties will affect the size and shape of the micelles formed.

Effect of pH. Micelles of the $(GVGVP)_{40}$-foldon are observed to form only above a pH of 9.6, while below this pH the polypeptide aggregates into larger unstable particles. This is above the pK_a of a typical N-terminal amine (about pH of 9). At pH values below this, protonation of the N-terminus results in positive charges on the ELP tails, giving a net charge to the ELP core, presumably disrupting micelle formation. At higher pH values, a higher fraction of the N-termini is neutral and aggregation of the ELP in the core of the micelle becomes energetically favorable.

One possible mechanism to explain the effect of pH changes on micelle size is the presence of end charges preventing the three arms from folding together, which then results in more extended chains of ELP in the micelle core. The micelle size reaches a plateau around a pH of 10.2, when the majority of N-terminal amines are deprotonated. The pK_a is the pH at which 50% of all the N-terminal amines are deprotonated. Therefore, at a pH of 9 there still would be a considerable number of charged N-terminal amines. On the other hand above a pH of about 10, we expect that nearly all of the N-terminal amines are uncharged.

Regime I. This regime occurs in solutions with a salt concentration of up to 15 mM, where a fairly constant diffusion coefficient is observed above the transition temperature (Figure 2). Below the transition temperature in this salt concentration regime DLS reveals two distinguishable modes. The diffusive mode was found to correspond to particles with a hydro-dynamic radius (R_h) of about 3−5.5 nm. This mode is consistent with the $(GVGVP)_{40}$-foldon trimers in a random coil

formation. The second mode observed below the transition was found to be nondiffusive and corresponds to much slower processes in the system such as relaxation of the unfolded trimers.

The single mode observed for the 10 mM salt above the transition was found to be diffusive (Figure 3a). This mode has properties of spherical particles with an apparent hydrodynamic radius of 13.2−15.5 nm, corresponding to micelles formed from folded $(GVGVP)_{40}$-foldon trimers. Since the viscosity of a solution is dependent on the hydrodynamic size of solutes, resulting data can be combined with the DLS results to gain a better picture of the micelles.

The viscometry results show that the density of the polypeptide within the hydrodynamic volume of the micelle is 0.302 g/cm^3. Combining this with the volume of the micelles calculated from the hydrodynamic radius (14 nm), one obtains a molecular weight for the micelles of 2090 kDa, corresponding to an aggregation number of 35 $(GVGVP)_{40}$-foldon trimers. The ELP which is in the core of the micelle is 38% of the total polypeptide weight, 1730 kDa or 2.88×10^{-18} g/micelle. As mentioned before, the phase-separated ELP forms a protein-rich phase, and assuming that it is the same as in bulk, the aggregated phase consists of 62% water for a total core mass of 7.78×10^{-18} g/micelle. With a density of ∼1.2 g/cm^3, the resulting radius of the spherical core is 11.6 nm.

The core of the micelle consists of aggregated ELP chains only, and the foldon head groups need to be added to calculate the actual size of the micelles. The average diameter of the foldon domain is about 2.8 nm, resulting in a total radius of 14.4 nm, slightly larger than the measured hydrodynamic diameter. This may indicate that the foldon is slightly embedded within the core. It is important to note that the volume of the 35 foldon domains is not sufficient to fill the outer volume, and so there must be additional surface water that is carried with the micelle (Figure 7).
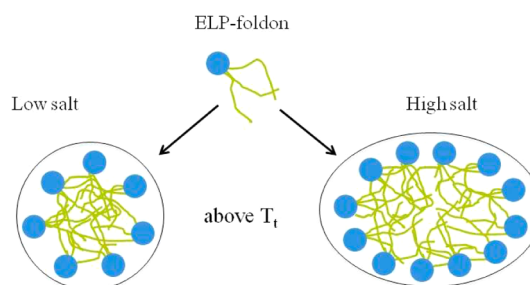

Figure 7. Schematic diagram of micelle formation above the transition temperature at low and high salt concentrations. Surface water makes the apparent diameter larger than the hydrodynamic diameter.

The molecular weight of the micelles measured by static light scattering gives a value of between 2700 and 3600 kDa. This is about 50% higher than the values from the values determined from DLS and viscometry. This discrepancy in the values could be the result of errors in the measurements. For the viscosity measurement it is estimated that there is up to 10% error, but since the errors are proportional to the error in the calculation of molecular weight, this would have a limited effect. However, the molecular weight calculation is more sensitive to the hydrodynamic radius from DLS, where a 10% increase in radius would bring the molecular weight up into the range of the SLS results.

The spherical geometry of micelles at low-salt concentrations is also consistent with the ordered (possibly β-spiral) structure of the ELP above the transition temperature.[13] The β-spiral of the $(GVGVP)_{40}$, which acts as the hydrophobic tail of the micelle construct, is considered to have a maximum length of about 15 nm. Since the maximum radius of a spherical micelle should not exceed the length of the hydrophobic tail, micelles of up to about 15 nm in radius are expected. This is consistent with the observed micelle radius which is somewhat smaller than the expected 15 nm in the low-salt regime. It is possible that the actual folded constructs of ELPs in the micelles are in a more compact form than the prediction of the molecular model.

Transition Region. The transition region starts around 15 mM salt, where the micelles begin to gradually increase in size, and continues to about 30 mM salt, when the size reaches a plateau. The decay rates of correlation functions in this region are slower than in the first salt regime, and the correlation functions are better fit to two distinct modes. While a jump in the micelle size above 15 mM was reported previously,[23] the transition region was not previously observed. The depolarized light scattering in this region produced only a weak signal which might be an indication of polydisperse scatterers with small optical anisotropy. SLS experiments in this region show significant linear angular dependence of $(I)^{-1/2}$, indicating that scattering species are big enough to show strong dependence on scattering angle in the studied q range. In this region, the particles become larger and the molecular weight increases up to about 60 000 kDa at the start of the second salt regime (Figure 4).

Regime II. This regime starts from a salt concentration of about 30 mM. The observed correlation functions have considerably slower decay rates than the correlation functions of regime I, corresponding to particles with bigger apparent size. This finding is in general agreement with our previous results.[23] Multiple scattering is unlikely as samples in this regime continue to be clear (as they are at lower salts) with no apparent tinge of blue observed. The correlation functions in this regime reveal two distinct modes. On the basis of the two-mode analysis of the correlation functions, the slow mode is consistently present in this concentration regime and constitutes about 50−60% of correlation function. The presence of the second mode either indicates significant geometrical anisotropy of micelles or hints at the presence of other slower processes such as the diffusion of random coils. In this salt regime the two modes should not be averaged as they exhibit a very different behavior, as is apparent from the different angular dependences of their corresponding decay rates (Figure 3c). The anisotropy of the micelles in this regime can also be seen from the somewhat nonlinear angular dependence of $(I)^{-1}$ (Zimm plot, see Supporting Information). The strongest proof of micellar anisotropy in this salt regime, however, comes from the strong depolarized (VH) scattering signal (Supporting Information). The reproducible strong VH scattering can be due to only two sources:[28] (a) the optical anisotropy of micelle building blocks or micelles themselves and (b) significant geometrical anisotropy of micelles. Since $(GVGVP)_{40}$-foldon trimers did not reveal any scattering signature of significant optical anisotropy below the transition and since spherical micelles formed at low salt concentration did not show any optical anisotropy, we can assume that the strong VH signal is due to nonspherical shape of micelles in this regime.

The observed increase in the molecular weight between salt regimes I and II from 2700−3500 kDa to 55 000−85 000 kDa is also in agreement with observations of micelles becoming anisotropic in the high-salt regime. It was found that the apparent molecular weight in regime II increases somewhat with rising salt concentration, potentially indicating further growth of micelle dimensions.

The effect of salt on micelles can be rationalized by considering the fact that at higher salt concentrations the head groups of trimers, which consist of a negatively charged foldon domain, become smaller. The shape of the micelles is directly affected by the packing factor, $V/a_0 l$, where V is the micelle volume, l is the length of the hydrophobic tail, and a_0 is the surface area of the headgroup. The smaller headgroup corresponds to a larger packing factor, and when it becomes larger than 1/3, the micelles begin to become nonspherical.[29] Consequently, in our system higher salt concentrations push the system toward nonspherical particles that can accommodate many more of the trimeric monomers, leading to a much higher molecular weight. These conclusions are in agreement with our SLS and DLS data and especially depolarized DLS data. It is possible that these elongated micelles have a distribution of different lengths and consequently a distribution of different molecular weights because one can expect very little energy barrier between formation of different lengths of elongated particles.

There is also a jump in the size deduced from the second mode in this regime around 45 mM of salt, which is consistent with the previously reported start of the third concentration regime.[23] This might be explained by the idea that at salt concentrations above 45 mM the micelle headgroup shrinks to such a small size that larger aggregates can start to grow.

Study of Micelle Elongation. Depolarized dynamic light scattering at different salt concentrations provided the best tool to study the anisotropy of the micelles under these conditions. The measured correlation functions from both VH and VV experiments showed strong angular dependence (Supporting Information). The decay rates of VV and VH correlation functions are shown as a Γ vs q^2 plot (Figure 5). Both VV and VH decay rates show a largely linear dependence on q^2 with similar slopes, which is especially true if only low-q VV data is considered. The VH measurements resulted in a somewhat more significant non-zero intercept than VV measurements. These findings are in agreement with eqs 6 and 7 according to which the slopes of Γ vs q^2 for both VV and VH should yield the translational diffusion coefficient while the intercept from the VH measurement is proportional to the rotational diffusion coefficient. A cylindrical model was used to calculate the elongation of the micelles at each salt concentration using measured translational and rotational diffusion coefficients. In this model we used a cylinder with diameter (d) equivalent to the maximum diameter of the spherical micelles (30 nm). The length (L) was calculated from D_T and θ_R using the Tirado model relations[30,31]

$$D_T = \frac{k_B T}{3\pi\eta L}[\delta + \gamma] \tag{11}$$

$$\theta_R = \frac{3k_B T}{\pi\eta L^3}(\delta + \xi) \tag{12}$$

in which

$$\delta = \ln \frac{L}{d} \qquad (13)$$

$$\gamma = 0.312 + \frac{0.565d}{L} - \frac{0.1d^2}{L^2} \qquad (14)$$

$$\xi = -0.662 + \frac{0.917d}{L} - \frac{0.05d^2}{L^2} \qquad (15)$$

where $k_B T$ is Boltzmann factor and η is the viscosity of the solvent.

By fitting the data from our DDLS experiments to this model the extent of elongation of the particles in each regime was calculated (Figure 8 and data in Supporting Information).
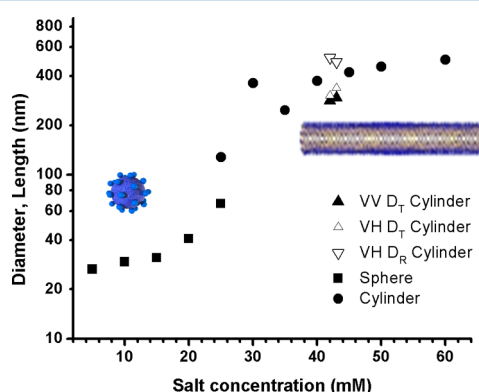

Figure 8. Diameter of spherical micelles (up to 25 mM of salt) and length of cylindrical micelles (at and above 25 mM) as a function of salt concentration from DLS and DDLS. Unpolarized DLS data up to 25 mM was analyzed using the spherical model (squares). DLS data at 25 mM and above was fit to the Tirado et al. cylindrical model (circles) using a cylinder diameter of 30 nm. Vertically (VV) and horizontally (VH) polarized DDLS data at two high-salt concentrations was also analyzed using the cylinder model for a 30 nm wide cylinder. Translational diffusion results appear as upward triangles. Rotational diffusion results appear as downward triangles.

Figure 8 shows the diameter of spherical micelles in regime I, both the diameter and the length of the micelles according to spherical and cylindrical models, respectively, in the transition region, and the length of the cylindrical micelles in regime II. In addition to the dimensions obtained from unpolarized DLS (black points), Figure 8 also shows the cylinder length obtained from DDLS data. The length was calculated separately from translational diffusion VV and VH data and rotational diffusion VH data. The agreement between results from two different translational diffusion sets of data is good; however, the rotational diffusion data gives somewhat larger cylinder lengths. Generally, the translational diffusion DDLS data gives somewhat smaller lengths than unpolarized data, while rotational diffusion data gives somewhat larger lengths. The potential source of disagreement between rotational and translational diffusion comes from the flexible nature of elongated micelles (in fact, the apparent persistence length of the micelles was estimated following ref 32 to be less than 105 nm, see Supporting Information) and/or from potential hydrodynamic interactions of micelles.

As for the dependence of micelle dimensions and geometry on salt concentration, again two regimes and the transition region can be identified from Figure 8. The micelles in regime I (up to 15 mM of salt) are shown to be spheres of up to 30 nm

in diameter. The micelles in regime II (above 30 mM) are shown to have significant anisotropy, which can be modeled by cylindrical particles with a diameter of 30 nm and length of about 250−500 nm.

Considering cylindrical micelles with a core diameter of around 24.8 nm and lengths of 250−420 nm (unpolarized DLS results), the number of trimers that are contained in these micelles is calculated to be 640−1100 based on the volume of 188 nm^3 for each trimer (62% water and density of 1.2 g/cm^3). This corresponds to molecular weights from 39 000 to 65 000 kDa (see Supporting Information). From SLS measurements the molecular weight of micelles in this regime is found to be between 55 000 and 85 000 kDa.

CONCLUSION

In this work, the geometry and size of thermoresponsive micelles made from three-armed star elastin-like polypeptides were investigated as a function of temperature, pH, and salt concentration. Studies were mainly based on using different light scattering techniques and also verified by viscosity measurements and TEM imaging. Temperature was shown to effectively drive the reversible micelle formation above the transition temperature of ELP. The solution pH was shown to be essential in micelle formation but also has a measurable effect on the size of the particles. While the micelles can only form in solutions above pH 9.6, they were shown to reach to a constant, minimum size at pH greater than 10.2. The effect of salt on the size of the micelles was divided into a low-salt regime (below 15 mM), high-salt regime (above 30 mM), and an intermediate region. Micelles in the low-salt regime were shown to be spherical and consisted of about 35 unimers, while micelles in the high-salt regime were found to be very elongated cylindrical particles with high molecular weights. The intrinsic viscosity was measured at temperatures above the transition to independently verify total mass and volume of the micelles at low salts. The electron microscopy verified the spherical nature of micelles at low-salt regime.

ASSOCIATED CONTENT

Supporting Information

Values of dn/dc; dependence of apparent D on pH, observed micelle correlation functions at different salt concentrations; Zimm and Berry plots of SLS data; table of R_g and R_h values; VH correlation functions at 42 mM; Intrinsic viscosity based on viscosity measurements at different concentrations; persistence length of micelles; table of salt concentration dependence of measured and calculated M and of size of micelles below and above the transition from polarized and unpolarized DLS data and TEM (at low-salt only); protein concentration dependence of micelle diffusion at 10 mM and 50 °C. This material is available free of charge via the Internet at http://pubs.acs.org.

AUTHOR INFORMATION

Corresponding Author

*E-mail: k.streletzky@csuohio.edu.

Notes

The authors declare no competing financial interest.

■ REFERENCES

(1) Duncan, R. The Dawning Era of Polymer Therapeutics. *Nat. Rev. Drug Discovery* **2003**, *2*, 347−360.

(2) Herrero-Vanrell, R.; Rincon, A. C.; Alonso, M.; Reboto, V.; Molina-Martinez, I. T.; Rodriguez-Cabello, J. C. Self-Assembled Particles of an Elastin-Like Polymer as Vehicles for Controlled Drug Release. *J. Controlled Release* **2005**, *102*, 113−122.

(3) Kakizawa, Y.; Kataoka, K. Block Copolymer Micelles for Delivery of Gene and Related Compounds. Adv. *Drug Delivery Rev.* **2002**, *54*, 203−222.

(4) Langer, R. Perspectives: Drug Delivery - Drugs on Target. *Science* **2001**, *293*, 58−59.

(5) Moghimi, S. M.; Hunter, A. C.; Murray, J. C. Long-Circulating and Target-Specific Nanoparticles: Theory to Practice. *Pharmacol. Rev.* **2001**, *53*, 283−318.

(6) Rapoport, N. Physical Stimuli-Responsive Polymeric Micelles for Anti-Cancer Drug Delivery. *Prog. Polym. Sci.* **2007**, *32*, 962−990.

(7) Kataoka, K.; Harada, A.; Nagasaki, Y. Block Copolymer Micelles for Drug Delivery: Design, Characterization and Biological Significance. *Adv. Drug Delivery Rev.* **2001**, *47*, 113−131.

(8) Nishiyama, N.; Kataoka, K. Current State, Achievements, and Future Prospects of Polymeric Micelles as Nanocarriers for Drug and Gene Delivery. *Pharmacol. Ther.* **2006**, *112*, 630−648.

(9) Gros, L.; Ringsdorf, H.; Schupp, H. Polymeric Anti-Tumor Agents on a Molecular and on a Cellular-Level. *Angew. Chem., Int. Ed. Engl.* **1981**, *20*, 305−325.

(10) Pratten, M. K.; Lloyd, J. B.; Horpel, G.; Ringsdorf, H. Micelle-Forming Block Copolymers - Pinocytosis by Macrophages and Interaction with Model Membranes. *Makromol. Chem.-Macromol. Chem. Phys.* **1985**, *186*, 725−733.

(11) Chen, T.; Guo, X.; Liu, X.; Shi, S.; Wang, J.; Shi, C.; Qian, Z.; Zhou, S. A Strategy in the Design of Micellar Shape for Cancer Therapy. *Adv. Healthcare Mater.* **2012**, *1*, 214−224.

(12) Urry, D. W.; Shaw, R. G.; Prasad, K. U. Polypentapeptide of Elastin - Temperature-Dependence of Ellipticity and Correlation with Elastomeric Force. *Biochem. Biophys. Res. Commun.* **1985**, *130*, 50−57.

(13) Urry, D. W. Physical Chemistry of Biological Free Energy Transduction as Demonstrated by Elastic Protein-Based Polymers. *J. Phys. Chem. B* **1997**, *101*, 11007−11028.

(14) Ghoorchian, A.; Holland, N. B. Molecular Architecture Influences the Thermally Induced Aggregation Behavior of Elastin-like Polypeptides. *Biomacromolecules* **2011**, *12*, 4022−4029.

(15) Meyer, D. E.; Chilkoti, A. Quantification of the Effects of Chain Length and Concentration on the Thermal Behavior of Elastin-Like Polypeptides. *Biomacromolecules* **2004**, *5*, 846−851.

(16) Urry, D. W.; Parker, T. M.; Reid, M. C.; Gowda, D. C. Biocompatibility of the Bioelastic Materials, Poly(GVGVP) and Its Gamma-Irradiation Cross-Linked Matrix - Summary of Generic Biological Test-Results. *J. Bioact. Compat. Polym.* **1991**, *6*, 263−282.

(17) Alonso, M.; Reboto, V.; Guiscardo, L.; Mate, V.; Rodriguez-Cabello, J. C. Novel Photoresponsive P-Phenylazobenzene Derivative of an Elastin-Like Polymer with Enhanced Control of Azobenzene Content and without pH Sensitiveness. *Macromolecules* **2001**, *34*, 8072−8077.

(18) Strzegowski, L. A.; Martinez, M. B.; Gowda, D. C.; Urry, D. W.; Tirrell, D. A. Photomodulation of the Inverse Temperature Transition of a Modified Elastin Poly(pentapeptide). *J. Am. Chem. Soc.* **1994**, *116*, 813−814.

(19) Valiaev, A.; Abu-Lail, N. I.; Lim, D. W.; Chilkoti, A.; Zauscher, S. Microcantilever Sensing and Actuation with End-Grafted Stimulus-Responsive Elastin-Like Polypeptides. *Langmuir* **2007**, *23*, 339−344.

(20) Chilkoti, A.; Dreher, M. R.; Meyer, D. E. Design of Thermally Responsive, Recombinant Polypeptide Carriers for Targeted Drug Delivery. *Adv. Drug Delivery Rev.* **2002**, *54*, 1093−1111.

(21) Dreher, M. R.; Simnick, A. J.; Fischer, K.; Smith, R. J.; Patel, A.; Schmidt, M.; Chilkoti, A. Temperature Triggered Self-Assembly of Polypeptides into Multivalent Spherical Micelles. *J. Am. Chem. Soc.* **2008**, *130*, 687−694.

(22) Fujita, Y.; Mie, M.; Kobatake, E. Construction of Nanoscale Protein Particle Using Temperature-Sensitive Elastin-Like Peptide and Polyaspartic Acid Chain. *Biomaterials* **2009**, *30*, 3450−3457.

(23) Ghoorchian, A.; Cole, J. T.; Holland, N. B. Thermoreversible Micelle Formation Using a Three-Armed Star Elastin-like Polypeptide. *Macromolecules* **2010**, *43*, 4340−4345.

(24) Streletzky, K. A.; McKenna, J. T.; Mohieddine, R. Spectral Time Moment Analysis of Microgel Structure and Dynamics. *J. Polym. Sci., Part B: Polym. Phys.* **2008**, *46*, 771−781.

(25) Phillies, G. D. J.; O'Connell, R.; Whitford, P.; Streletzky, K. A. Mode Structure of Diffusive Transport in Hydroxypropylcellulose: Water. *J. Chem. Phys.* **2003**, *119*, 9903−9913.

(26) Phillies, G. D. J.; Streletzky, K. A. Dynamics of Semirigid Rod Polymers from Experimental Studies. In *Soft Condensed Matter: New Research*; Dillon, K., Ed.; Nova Science: New York, 2007.

(27) Sperling, L. H. *Introduction to Physical Polymer Science*, 4th ed.; Wiley-Interscience: New York, 2006.

(28) Schillen, K.; Brown, W.; Johnsen, R. M. Micellar Sphere-to-Rod Transition in an Aqueous Triblock Copolymer System - A Dynamic Light-Scattering Study of Translational and Rotational Diffusion. *Macromolecules* **1994**, *27*, 4825−4832.

(29) Israelachvili, J.; Mitchell, J.; Ninham, B. Theory of Self-assembly of Hydrocarbon Amphiphiles into Micelles and Bilayers. *J. Chem. Soc., Faraday Trans. 2* **1976**, *72*, 1525−1568.

(30) Tirado, M. M.; Garciadelatorre, J. Rotational-Dynamics of Rigid, Symmetric Top Macromolecules - Application to Circular-Cylinders. *J. Chem. Phys.* **1980**, *73*, 1986−1993.

(31) Tirado, M. M.; Martinez, C. L.; Delatorre, J. G. Comparison of Theories for the Translational and Rotational Diffusion-Coefficients of Rod-Like Macromolecules - Application to Short DNA Fragments. *J. Chem. Phys.* **1984**, *81*, 2047−2052.

(32) Guerin, G.; Raes, J.; Manners, I.; Winnik, M. Light Scattering Study of Rigid, Rodlike Organometallic Block Copolymer Micelles in Dilute Solution. *Macromolecules* **2005**, *38*, 7819−7827.